

First-Principles Study on the Structural and Magnetic Properties of Low-Index Cu_2O and CuO Surfaces

Stefanie E. Bogenrieder, Julian Beßner, Albert K. Engstfeld, and Timo Jacob*

Cite This: <https://doi.org/10.1021/acs.jpcc.4c01102>

Read Online

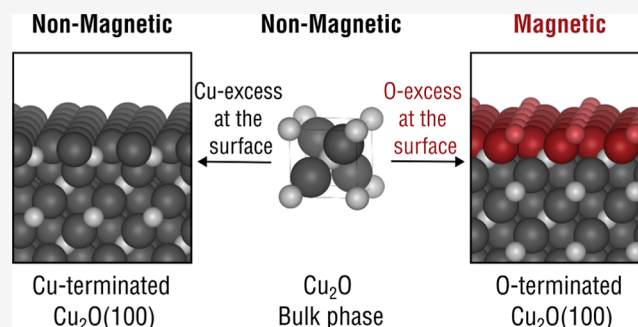
ACCESS |

Metrics & More

Article Recommendations

Supporting Information

ABSTRACT: Copper oxides play a crucial role in a wide range of research areas, such as catalysis, photocatalysis, sensing, energy storage, biomedicine, and spintronics. However, further insights into the surface structure and the related magnetic properties of copper oxides are required to improve their performance. Here, we present a computational study on the structural and magnetic properties of low-index Cu_2O and CuO surfaces including their bulk oxides based on spin-polarized density functional theory (DFT) via DFT + U and the ab initio atomistic thermodynamics approach. We found that Cu_2O surfaces with an excess of oxygen atoms show surface ferromagnetism, while CuO surfaces with an excess of copper atoms exhibit surface atoms without a magnetic moment. By analyzing the density of states and the Bader charges of the copper oxide surfaces and the origin of the observed magnetism. Finally, we derive a correlation between the structure and the magnetic properties of copper oxide surfaces and suggest a possible explanation for the observed magnetism within a simplified model.



INTRODUCTION

The remarkable electrical, optical, thermal, antimicrobial, and magnetic properties, as well as the nontoxicity and low cost establish copper oxides as crucial materials in a wide range of fields, including catalysis, photocatalysis, sensing, energy storage, biomedicine, and spintronics.^{1–6} Due to these properties and the broad range of applications, copper oxides are among the most intensively studied binary oxides.⁷ Accordingly, several overviews on the vast field of research on copper oxides have been published and can be found elsewhere.^{1–11} In the present work, we focus on the relationship between the surface structure and magnetic behavior of copper oxide surfaces and aim to provide a foundation for future investigations of catalytic reactions on these surfaces.

Cu_2O and CuO are p -type semiconductors with relatively narrow band gap energies (2.0–2.2 eV for Cu_2O and 1.2–1.9 eV for CuO),¹² which makes them particularly interesting as catalysts in photoelectrochemical reduction reactions, such as the CO_2 reduction reaction (CO_2RR) and the nitrogen reduction reaction (NRR).^{2,13} Furthermore, Cu_2O and CuO are $3d$ transition metal oxides and as such have unique magnetic properties. While Cu_2O has a diamagnetic (DM) and CuO an antiferromagnetic (AFM) ground state, their surfaces exhibit different types of magnetism.^{14–23} For example, room-temperature ferromagnetic (FM) properties of Cu_2O microcrystals,¹⁵ room-temperature ferromagnetism in pure CuO nanoparticles,¹⁸ and size effects on the magnetic properties of Cu_2O and CuO nanoparticles have been reported experimentally.^{14,21}

Although several studies have identified different types of magnetism in copper oxide nanoparticles, the origin of the observed surface magnetism is still not fully understood. Experimental and theoretical reports suggested that the wide spectrum of magnetic properties may originate from defects such as cation and/or oxygen vacancies.^{15,16,18,21,24} In contrast, a theoretical study by Yu et al. revealed that some terminations of low-index Cu_2O surfaces exhibit surface ferromagnetism without the presence of defects.¹⁷ According to their work, the origin of the surface ferromagnetism of Cu_2O can be understood within the framework of Stoner's theory and may be due to the more pronounced $2p$ - $3d$ hybridization of surface Cu and O atoms compared with atoms underneath.¹⁷ However, it remains unclear why some terminations of the low-index Cu_2O surfaces exhibit surface ferromagnetism while others do not and how the surface magnetism of copper oxides relates to their surface structure in general.

The structure and stability of different terminated stoichiometric Cu_2O and CuO surfaces and nonstoichiometric Cu_2O surfaces have previously been investigated.^{22,24–28} Soon et al.

Received: February 20, 2024

Revised: April 18, 2024

Accepted: May 20, 2024

Table 1. Lattice Parameters (a , b , c , and β), Energy of Formation $\Delta_f G^\circ$ ($T = 0$ K), Magnetic Moment m_B of the Cu Atoms, and Band Gap E_G for Cu_2O and CuO from PBE + U Calculations Compared to Experimental Data

oxide	method	a [Å]	b [Å]	c [Å]	β [°]	$\Delta_f G^\circ$ [eV atom ⁻¹]	m_B [μ_B]	E_G [eV]
Cu_2O	PBE + U	4.28	4.28	4.28	90.0	-0.58	0.00 (DM)	0.8
	Exp. ^{12,43}	4.27	4.27	4.27	90.0	-0.58	0.00 (DM)	2.0–2.2
CuO	PBE + U	4.66	3.48	5.15	97.8	-0.81	0.69 (AFM)	1.7
	Exp. ^{12,43}	4.68	3.42	5.13	99.5	-0.80	0.68 (AFM)	1.2–1.9

and Bendavid et al. described the surface structure of different terminated low-index Cu_2O surfaces and calculated their surface energies as a function of the oxygen chemical potential.^{25,26,29} They found that the $\text{Cu}_2\text{O}(110)$ surface, terminated with both Cu and O atoms ($\text{Cu}_2\text{O}(110):\text{Cu}/\text{O}$), and the $\text{Cu}_2\text{O}(111)$ surface, containing a surface Cu vacancy ($\text{Cu}_2\text{O}(111)-\text{Cu}_{\text{cus}}$), are energetically most favorable.^{25,26,29}

In the case of CuO , the stoichiometric $\text{CuO}(111):\text{Cu}/\text{O}$ surface has been identified as the most stable CuO surface by Hu et al. and Mishra et al.^{22,28} To our knowledge, there are no theoretical reports on the structure and stability of polar nonstoichiometric CuO surfaces.

Although the surface structure appears to have a significant influence on the magnetic behavior of copper oxide surfaces, the precise nature of this relationship is not yet fully understood.^{17,23,24} Especially in the field of spintronics, it is of great interest to understand the magnetic properties of nanocrystalline magnetic semiconductors, such as nanosized copper oxides.³⁰ Therefore, further insights into the surface structure and the associated magnetism of copper oxides are needed to improve their performance for many applications.

In this systematic study, we present detailed insights into the structural and magnetic properties of different terminated low-index Cu_2O and CuO surfaces and derive a correlation between their surface structure and magnetic behavior. Furthermore, we analyze the electronic properties of these surfaces through spin-polarized density of states (DOS) calculations and a Bader charge analysis to investigate the origin of the observed surface magnetism. Within the framework of a simplified model, we discuss why some terminations of the low-index Cu_2O surfaces exhibit surface ferromagnetism while others do not and how the surface magnetism of copper oxides relates to their surface structure in general.

METHODS

All calculations were performed using density functional theory (DFT) implemented in the plane-wave-based Vienna ab initio simulation package (VASP).^{31,32} Electron–core interactions were described by the projector augmented wave (PAW)^{33,34} method. The generalized gradient approximation (GGA) according to Perdew, Burke, and Ernzerhof (PBE)³⁵ was employed as the exchange–correlation functional. In order to describe the magnetic properties of Cu_2O and CuO , spin polarization was included for all cases, and the Hubbard parameter, U , was applied to all Cu $3d$ electrons according to Dudarev et al.³⁶ Using this PBE + U method, the lattice parameter, energy of formation, magnetic moment, and band gap of Cu_2O and CuO were investigated for various values of the Hubbard U parameter and compared to experimental data, as shown in the Supporting Information (Table S1). The closest representation of the experimental results shown in Tables 1 and S1 was obtained for a common U value of 8 eV, and therefore this value was used for all subsequent calculations. The same

value was obtained by Zivkovic et al., who also performed a systematic study to determine the U value for copper oxides.³⁷

For the Cu_2O and CuO bulk phases, a plane-wave cutoff energy of 550 eV was applied using Gaussian smearing with a width of 0.05 eV. The Brillouin zone was sampled using a $12 \times 12 \times 12$ Monkhorst–Pack³⁸ k -point grid for Cu_2O and a $10 \times 14 \times 10$ grid for CuO . The structure relaxations were assumed to be converged when the energy differences of the electronic self-consistent field (SCF) were smaller than 10^{-5} eV and all forces were at least smaller than $1.0 \text{ meV } \text{Å}^{-1}$.

Based on the optimized bulk structures, symmetric slabs with two identical surfaces were modeled for all possible terminations of the low-index (100), (110), and (111) surfaces of Cu_2O and CuO . For all surfaces, the surface energy was calculated for slabs with different thicknesses and was assumed to be converged when the difference in surface energy was smaller than $1.0 \text{ meV } \text{Å}^{-2}$. Based on these results, we chose a slab thickness between 17 and 21 Å, depending on the respective surface. In order to avoid interactions between the periodic slabs in the z direction, a vacuum region of 20 Å was added in all cases. For the surface calculations, the plane-wave cutoff energy was set to 500 eV, and Gaussian smearing was applied with a width of 0.05 eV. The atomic position of every atom was fully relaxed until the Hellmann–Feynman forces were smaller than $1.0 \text{ meV } \text{Å}^{-1}$ and the energy difference of consecutive SCF cycles was smaller than 10^{-5} eV. The Brillouin zone was sampled using Γ -centered Monkhorst–Pack³⁸ k -point grids of $9 \times 9 \times 1$, $9 \times 7 \times 1$, $7 \times 7 \times 1$, $11 \times 7 \times 1$, $7 \times 7 \times 1$, and $7 \times 7 \times 1$ for $\text{Cu}_2\text{O}(100)$, $\text{Cu}_2\text{O}(110)$, $\text{Cu}_2\text{O}(111)$, $\text{CuO}(100)$, $\text{CuO}(110)$, and $\text{CuO}(111)$, respectively.

To achieve high precision DOS calculations, the convergence criterion for the SCF cycle was decreased to 10^{-8} eV and the density of the k -point mesh was increased significantly (at least doubled). The VASPKIT³⁹ package was used to postprocess the DOS calculations. The charge on atoms was calculated using the Bader charge analysis,^{40,41} and crystal structure drawings were visualized using VESTA.⁴²

RESULTS AND DISCUSSION

Bulk Properties. Cuprous oxide (Cu_2O) crystallizes in a primitive cubic Bravais lattice (space group Pn3m). The unit cell, shown in Figure 1 (left), consists of two formula units, i.e., four Cu and two O atoms. The Cu atoms (large dark gray spheres) are linearly coordinated to two O atoms (small light gray spheres) and arranged in a face-centered cubic (fcc) sublattice, while each O atom is tetrahedrally coordinated with four Cu atoms, forming a body-centered cubic (bcc) sublattice. Both types of atoms in Cu_2O have no local magnetic moment. Thus, the material is DM.

As shown in Table 1, the calculated lattice parameters, energy of formation $\Delta_f G^\circ$, and magnetic structure (DM) are in excellent agreement with the experimental results.^{12,43} However, the band gap E_G of Cu_2O is underestimated, which is well-known for

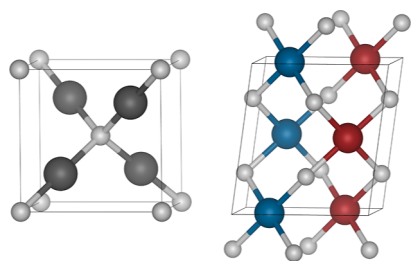


Figure 1. Crystal structure of cuprous oxide, Cu_2O (left), and cupric oxide, CuO (right). Oxygen and copper atoms without a magnetic moment are shown in light and dark gray, respectively. Copper atoms with a magnetic moment are illustrated in red (up) or blue (down) depending on the orientation of the local magnetic moments.

standard DFT and has already been discussed elsewhere.^{12,44} The calculated Cu–O bond length, $d_{\text{Cu-O}}$, and Cu–Cu distance, $d_{\text{Cu-Cu}}$ are 1.853 Å [expt. 1.849 Å]⁴⁵ and 3.027 Å [expt. 3.012 Å],⁴⁵ respectively. These values deviate by less than 0.5% from the experimental values.

In contrast, cupric oxide, CuO , crystallizes in a base-centered monoclinic Bravais lattice (space group $C2/c$). The CuO unit cell contains eight atoms: four Cu and four O atoms. As shown in Figure 1 (right), each Cu atom (large blue or red spheres) is coordinated with four O atoms (small light gray spheres) in an approximately square planar configuration, and each O atom forms a distorted tetrahedron with four Cu atoms. Below the Néel temperature of 230 K, CuO is AFM, and the local magnetic moments of the Cu atoms are aligned parallel to the monoclinic b axis,⁴⁶ as shown in Figure 1. Additional AFM configurations with different arrangements of the magnetic moments were investigated and are shown in the Supporting Information (Figure S1). Although the energies of formation of these AFM configurations are very similar, the magnetic structure observed experimentally (Figure 1) is also the most stable in our study. Therefore, this configuration was subsequently considered in more detail.

Similar to Cu_2O , the calculated lattice parameters, energy of formation $\Delta_f G^\circ$, magnetic moment m_B of the Cu atoms, and the magnetic structure (AFM) for CuO are in good agreement with the experimental results, as summarized in Table 1. Only the lattice angle β of CuO is slightly underestimated compared to the experimental value. Furthermore, the calculated distances of 1.96 Å [expt. 1.96 Å]⁴⁵ for $d_{\text{Cu-O}}$ and 2.91 Å [expt. 2.90 Å]⁴⁵ for $d_{\text{Cu-Cu}}$ deviate by less than 0.4% from the experimental values. In contrast to Cu_2O , the calculated band gap E_G of 1.7 eV for CuO is in excellent agreement with the experimental results, which vary between 1.2 and 1.9 eV, depending on the sample preparation and the employed measurement techniques.¹²

Comparing the bulk structures of the two copper oxides, the question arises: How can the different magnetic structures of Cu_2O and CuO be explained? Assuming an ionic nature of the Cu–O bonds, in Cu_2O , each Cu atom has an oxidation state of +1 with an electron configuration of $[\text{Ar}]3d^{10}$. Thus, the Cu ions have no unpaired 3d electrons and, therefore, have no local magnetic moments. In turn, in CuO , the Cu atoms have an oxidation state of +2 with an electron configuration of $[\text{Ar}]3d^9$. Thus, these Cu ions have unpaired 3d electrons, leading to local magnetic moments. Based on this assumption (the ionic nature of the Cu–O bonds), it can therefore be deduced why Cu_2O is DM and CuO is not. Furthermore, we expect that the phenomenon of antiferromagnetism in CuO can be explained by the so-called superexchange interaction. Here, the unpaired

Cu-3d electrons interact with O-2p electrons, which leads to a spin correlation between neighboring Cu^{2+} ions. This indirect interaction between neighboring Cu ions via the interjacent O ion leads to an AFM arrangement of the local magnetic moments and is also observed in other transition metal oxides.⁴⁷ These assumptions agree with the performed DOS calculations and the Bader charge analysis, which are shown in the Supporting Information (Figure S2 and Table S2). While the DOS calculations indicate a $2p\text{-}3d$ hybridization between the O and Cu atoms, the Bader charge analysis suggests that the Cu–O bond has both an ionic and a covalent character.

Low-Index Cu_2O Surfaces. Surface Structures. The low-index (100), (110), and (111) surfaces of Cu_2O were investigated, considering all possible surface terminations. The fully relaxed surfaces are shown in Figure 2 and, in addition, in a slightly different perspective in the Supporting Information (Figure S3).

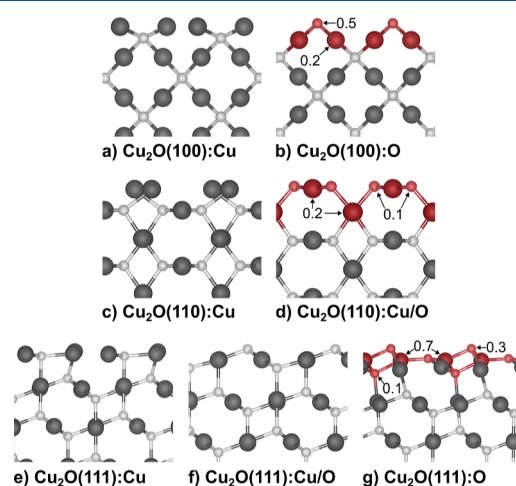


Figure 2. Side views of the calculated low-index Cu_2O surfaces in their corresponding most stable magnetic structure. (a) $\text{Cu}_2\text{O}(100):\text{Cu}$, (b) $\text{Cu}_2\text{O}(100):\text{O}$, (c) $\text{Cu}_2\text{O}(110):\text{Cu}$, (d) $\text{Cu}_2\text{O}(110):\text{Cu/O}$, (e) $\text{Cu}_2\text{O}(111):\text{Cu}$, (f) $\text{Cu}_2\text{O}(111):\text{Cu/O}$, and (g) $\text{Cu}_2\text{O}(111):\text{O}$. Oxygen and copper atoms without a magnetic moment are shown in light and dark gray, respectively. Oxygen and copper atoms with local magnetic moments in the same direction (up) are shown in light and dark red.

For the (100) surface, the outermost atomic layer can consist of either Cu or O atoms. On the Cu-terminated $\text{Cu}_2\text{O}(100):\text{Cu}$ surface, shown in Figure 2a, the outermost Cu atoms are only coordinated with one O atom instead of two as in the bulk phase. These coordinatively unsaturated Cu atoms form Cu–Cu dimers at the surface, where the Cu–Cu distance $d_{\text{Cu-Cu}}$ is reduced by 20% (2.41 Å) compared to the bulk distance. In turn, the Cu–O bond is elongated by 4% (1.93 Å) compared to the Cu–O bonds in the bulk. On the O-terminated $\text{Cu}_2\text{O}(100):\text{O}$ surface, the O atoms on the surface are coordinated with only two Cu atoms, which is shown in Figure 2b. The coordinatively unsaturated O atoms are located closer to the neighboring Cu atoms, which leads to a shortening of the Cu–O bond by 6% (1.75 Å) compared to those in the Cu_2O bulk. In comparison to the Cu-terminated surface, only moderate relaxation effects were observed for the O-terminated surface.

The (110) surface of Cu_2O consists of alternating CuO and Cu layers. Therefore, there are two possible surface terminations: the Cu-terminated $\text{Cu}_2\text{O}(110):\text{Cu}$ surface and

the Cu/O-terminated $\text{Cu}_2\text{O}(110):\text{Cu}/\text{O}$ surface. Similar to the $\text{Cu}_2\text{O}(100):\text{Cu}$ surface, the outermost Cu atoms on the $\text{Cu}_2\text{O}(110):\text{Cu}$ surface are bound to only one O atom and are, therefore, coordinatively unsaturated. This leads to a relaxation of the first Cu layer, as presented in Figure 2c, and a lengthening of the Cu–O bond by 4% (1.93 Å) compared to that in the respective bulk phase. The outermost layer of the $\text{Cu}_2\text{O}(110):\text{Cu}/\text{O}$ surface contains coordinatively saturated Cu atoms and coordinatively unsaturated O atoms, as shown in Figure 2d. Similar to the $\text{Cu}_2\text{O}(100):\text{O}$ surface, only moderate relaxation effects are apparent, resulting in a shortening of the Cu–O bond by 2% (1.81 Å) compared to those in the bulk.

On the (111) surface, three terminations are possible: the Cu-terminated $\text{Cu}_2\text{O}(111):\text{Cu}$, the Cu/O-terminated $\text{Cu}_2\text{O}(111):\text{Cu}/\text{O}$, and the O-terminated $\text{Cu}_2\text{O}(111):\text{O}$ surfaces. On the $\text{Cu}_2\text{O}(111):\text{Cu}$ surface, shown in Figure 2e, the outermost Cu atoms are coordinatively unsaturated, with a Cu–O bond distance of 2.00 or 2.02 Å (9% elongation compared to those in the bulk). On the stoichiometric $\text{Cu}_2\text{O}(111):\text{Cu}/\text{O}$ surface, shown in Figure 2f, the outermost O atoms are only coordinated to three Cu atoms. The outermost Cu atoms are bound to either one or two O atoms, with a 3:1 ratio of coordinatively saturated to unsaturated Cu atoms. Only minor surface relaxation was observed for this surface, resulting in a shortening of the Cu–O bond by less than 2% (1.82 Å) compared to those in the bulk. The O-terminated $\text{Cu}_2\text{O}(111):\text{O}$ surface undergoes surface reconstruction, as illustrated in Figure 2g. This reconstruction leads to coordinatively supersaturated Cu atoms on the surface with three Cu–O bonds instead of two. Similar to the $\text{Cu}_2\text{O}(111):\text{Cu}/\text{O}$ surface, the outermost O atoms of the $\text{Cu}_2\text{O}(111):\text{O}$ surface are coordinated to three Cu atoms, while coordinated saturated Cu atoms are also present on these surfaces. Due to the surface reconstruction, the Cu–O bond distances on the surface vary from 1.80 to 1.90 Å. In addition to the relaxation on the surface, contraction along the surface normal is observed in all cases, where the outermost layer moves closer to the layers below.

The calculated structural properties of the low-index Cu_2O surfaces agree well with those reported by Soon et al.²⁵ The main differences are minor variations within the bond lengths. The fundamental structures of the Cu_2O surfaces are also in good agreement with the study by Yu et al.,¹⁷ apart from the $\text{Cu}_2\text{O}(111):\text{O}$ surface. For this surface, we observed a surface reconstruction, whereas Yu et al.¹⁷ reported only small changes in bond lengths on the surface. A possible explanation for this discrepancy could be that we used more rigorous convergence criteria for the geometry optimizations, e.g., 0.001 eV Å⁻¹ instead of 0.02 eV Å⁻¹.¹⁷

Surface Magnetism. Except for the stoichiometric $\text{Cu}_2\text{O}(111):\text{Cu}/\text{O}$ surface, all Cu_2O surfaces have either an excess of Cu or O atoms on the surface and are therefore considered polar surfaces.²⁵ The excess of Cu or O atoms can be described with the stoichiometric ratio $R_{\text{Cu}/\text{O}} = N_{\text{Cu}}/N_{\text{O}}$, which is the ratio of the number of Cu atoms to the number of O atoms in the calculated cell. The corresponding values of $R_{\text{Cu}/\text{O}}$ for all calculated surfaces are given in Table 2. For the Cu_2O surfaces, values larger than two indicate an excess of Cu atoms, and values smaller than two indicate an excess of O atoms on the surface.

It seems that the stoichiometric ratio $R_{\text{Cu}/\text{O}}$ is correlated with the magnetic moments of the surface atoms, which are included in Figure 2. For surfaces with an excess of Cu atoms, such as $\text{Cu}_2\text{O}(100):\text{Cu}$, $\text{Cu}_2\text{O}(110):\text{Cu}$, and $\text{Cu}_2\text{O}(111):\text{Cu}$, as well as

Table 2. Stoichiometric Ratio $R_{\text{Cu}/\text{O}}$ and Surface Energies γ of Cu_2O and CuO Surfaces in Their Most Stable Magnetic Configurations under Oxygen-Poor (O-Poor) and Oxygen-Rich (O-Rich) Conditions^a

oxide	surface	termination	mag.	$R_{\text{Cu}/\text{O}}$	γ [meV Å ⁻²]	
					O-poor	O-rich
Cu_2O	100	Cu	DM	2.2	88	135
		O	FM	1.8	99	51
		Cu/O	FM	1.9	54	20
	110	Cu	DM	2.2	92	126
		Cu/O	DM	2.3	76	131
		Cu/O	DM	2.0	45	45
CuO	100	Cu	AFM	1.1	93	184
		O	AFM	0.9	214	124
		Cu/O	AFM	0.9	114	60
	110	Cu	AFM	1.1	66	120
		Cu/O	AFM	0.9	114	60
		Cu/O	AFM	1.0	45	45
111	Cu	AFM	1.1	114	207	
	Cu/O	AFM	1.0	45	45	
	O	AFM	0.9	226	134	

^a $R_{\text{Cu}/\text{O}}$ is the ratio of the number of Cu atoms to the number of oxygen atoms in the calculated cell.

the stoichiometric $\text{Cu}_2\text{O}(111):\text{Cu}/\text{O}$ surface (i.e., $R_{\text{Cu}/\text{O}} \geq 2$), the surface atoms do not have a magnetic moment. Therefore, the respective surfaces are DM as the Cu_2O oxide itself. However, for surfaces with an excess of O atoms (i.e., $R_{\text{Cu}/\text{O}} < 2$), such as $\text{Cu}_2\text{O}(100):\text{O}$, $\text{Cu}_2\text{O}(110):\text{Cu}/\text{O}$, and $\text{Cu}_2\text{O}(111):\text{O}$, the surface atoms have a magnetic moment.

Depending on the arrangement of these magnetic moments, different magnetic structures can occur. Figure 3 shows the

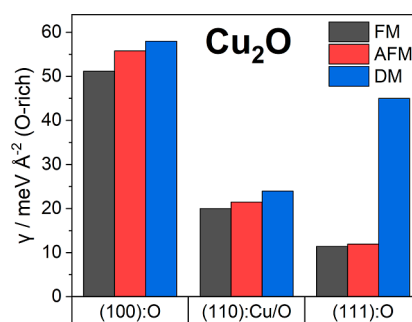


Figure 3. Surface energy for different magnetic structures of the $\text{Cu}_2\text{O}(100):\text{O}$, $\text{Cu}_2\text{O}(110):\text{Cu}/\text{O}$, and $\text{Cu}_2\text{O}(111):\text{O}$ surfaces. The FM, AFM, and DM configurations are indicated in black, red, and blue, respectively.

surface energies of the Cu_2O surfaces with an excess of O atoms for the FM, DM, and most stable AFM configurations, respectively. The corresponding surface structures within their most stable magnetic configuration are shown in Figure 2.

According to Figure 3, for all surfaces with an excess of O atoms, the FM configuration has the lowest surface energy and is, therefore, the most stable one. The AFM structure is the second-most stable for all of these surfaces, while the DM structure is the least stable. For the $\text{Cu}_2\text{O}(111):\text{O}$ surface, the surface energy difference between the FM and AFM structures is subtle, indicating that both structures are almost equally stable. However, the respective FM structure has the lowest surface energy for all O-excess Cu_2O surfaces and is, therefore, included in Figure 2 and described in more detail below.

As shown in Figure 2, the outermost atoms of the FM $\text{Cu}_2\text{O}(100):\text{O}$ surface have a magnetic moment of $0.5 \mu_{\text{B}}$ per O and $0.2 \mu_{\text{B}}$ per Cu atom, which are oriented in the same direction. For the FM $\text{Cu}_2\text{O}(110):\text{Cu}/\text{O}$ surface, the O atoms have a magnetic moment of $0.1 \mu_{\text{B}}$, while the Cu atoms in the two outermost Cu-layers have a magnetic moment of $0.2 \mu_{\text{B}}$. On the $\text{Cu}_2\text{O}(111):\text{O}$ surface, only the coordinatively super-saturated Cu atoms, which are coordinated to three O atoms, have a magnetic moment of $0.7 \mu_{\text{B}}$. The O atoms on this surface have a magnetic moment of $0.3 \mu_{\text{B}}$ or $0.1 \mu_{\text{B}}$ depending on their position in the z -direction. The more exposed the O atoms are on this surface, the higher their magnetic moment.

The surface ferromagnetism of Cu_2O was previously reported in theoretical studies.^{17,24} According to Yu et al., the Cu_2O bulk phase as well as the Cu/O-terminated $\text{Cu}_2\text{O}(111)$ and $\text{Cu}_2\text{O}(110)$ surfaces are not magnetic, while the O-terminated $\text{Cu}_2\text{O}(111)$ and the $\text{Cu}_2\text{O}(100)$ surfaces are magnetic.¹⁷ This is in good agreement with our study, except for the Cu/O-terminated $\text{Cu}_2\text{O}(110)$ surface, which exhibits surface ferromagnetism in our calculations. Soon et al. have also reported that the $\text{Cu}_2\text{O}(110):\text{Cu}/\text{O}$ surface is nonmagnetic.²⁴ However, according to our DFT + U calculations, the surface atoms of $\text{Cu}_2\text{O}(110):\text{Cu}/\text{O}$ indeed have a magnetic moment, as described above. Furthermore, we were able to identify distinct magnetic structures and compare their surface energies. In addition to theoretical calculations, experiments have also confirmed a FM behavior of Cu_2O nanospheres at 5 K,¹⁶ room-temperature ferromagnetism in Cu_2O nanowires,⁴⁸ and room-temperature FM behavior in Cu_2O microcrystals.¹⁵ Furthermore, other materials that are otherwise nonmagnetic, such as MoO_2 , Al_2O_3 , and ZnO , have been reported to exhibit surface ferromagnetism.^{49,50}

Electronic Properties. To gain a better understanding of the observed surface ferromagnetism, we calculated the spin-polarized DOS for all Cu_2O surfaces. The total, partial, and projected DOS of the $\text{Cu}_2\text{O}(100):\text{O}$ surface is shown in Figure 4, while the DOS for the other surfaces is given in the Supporting Information (Figures S4 and S5). For the $\text{Cu}_2\text{O}(100):\text{O}$ surface, there is a difference between the DOS for spin-up electrons (plotted upward) and the DOS for spin-down electrons (plotted downward), which is particularly pronounced in the vicinity of the Fermi level. This region is marked by an arrow and is illustrated with higher magnification in the inset of Figure 4.

The spin-up states of the valence band are fully occupied, while the spin-down states intersect the Fermi level, indicating partial occupancy and half-metallic behavior. These spin-down states near the Fermi level can be assigned to the surface atoms (outermost atomic layers) and have both Cu-3d and O-2p characters with similar density contributions, as shown by the partial and projected DOS. This 2p-3d hybridization can be observed not only for the surface atoms but also for the bulk-like atoms. The projected DOS shows that the states from -2.5 eV to the valence band maximum have both O-2p and Cu-3d contributions, while the states between -4 and -2.5 eV are almost exclusively related to Cu-d orbitals.

The other surfaces with an excess of O atoms (Figure S4) also show differences between the DOS for spin-up and spin-down electrons. For the $\text{Cu}_2\text{O}(110):\text{Cu}/\text{O}$ surface, this deviation is also most pronounced at the valence band maximum, while for the $\text{Cu}_2\text{O}(111):\text{O}$ surface, the most significant deviation is apparent at the conduction band minimum. However, the DOS for the surfaces with an excess of Cu atoms (Figure S5), as well as for the Cu_2O bulk (Figure S2), shows a nearly identical shape for

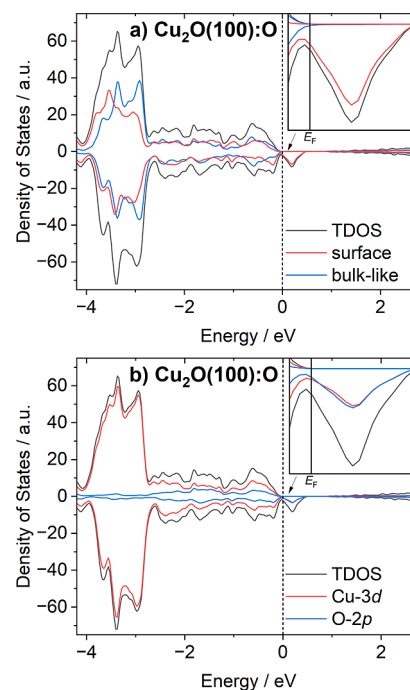


Figure 4. Partial (a) and projected (b) DOS of the $\text{Cu}_2\text{O}(100):\text{O}$ surface. The total DOS (TDOS) is shown in gray. The contribution of the surface atoms (outermost atom layers) and the Cu-3d orbitals are shown in red, while the contribution of all other (bulk-like) atoms in the calculated cell and the O-2p orbitals are represented in blue. The Fermi energy is indicated by a vertical dashed black line at 0 eV.

spin-up and spin-down states and, accordingly, no spin polarization.

For the O-terminated $\text{Cu}_2\text{O}(100)$ and $\text{Cu}_2\text{O}(111)$ surfaces, the difference between the DOS for spin-up and spin-down electrons was reported previously.¹⁷ In addition, half-metallic behavior has been observed for certain Cu_2O surfaces²⁴ and for bulk Cu_2O with cation vacancies.¹⁶

To gain further insight into the origin of the observed surface magnetism, we additionally performed a Bader charge analysis on all investigated systems. The respective Bader net atomic charges for the Cu- and O-terminated $\text{Cu}_2\text{O}(100)$ surfaces are illustrated in Figure 5. For both terminations, the charge of the atoms inside the slabs matches the charge of the respective

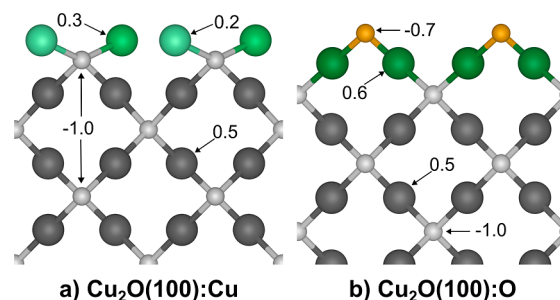


Figure 5. Side views of the $\text{Cu}_2\text{O}(100):\text{Cu}$ (left) and $\text{Cu}_2\text{O}(100):\text{O}$ (right) surfaces. The numbers refer to the Bader net atomic charges of the respective atoms. Oxygen and copper atoms with a net atomic charge similar to that of the Cu_2O bulk are shown in light and dark gray, respectively. Oxygen and copper atoms with a different net atomic charge compared to that of the bulk are shown in green (positive) and yellow (negative).

atoms in the bulk phase, i.e., 0.5 e for Cu and -1.0 e for O atoms, respectively. In the bulk as well as inside the slabs, each Cu atom is coordinated with two O atoms, while each O atom is coordinated with four Cu atoms. This indicates that on average 0.25 e is transferred from each Cu atom to each neighboring O atom. However, at the Cu-terminated $\text{Cu}_2\text{O}(100):\text{Cu}$ surface, the calculated Bader charges are 0.2 or 0.3 e for the outermost Cu atoms and -1.0 e for the outermost O atoms, as shown in Figure 5. This indicates that the coordinatively saturated outermost O atoms receive the same amount of charge as those in the bulk, while the coordinatively unsaturated outermost Cu atoms only transfer about half as much charge as those in the bulk. In other words, more electrons are localized on the outermost Cu atoms of the $\text{Cu}_2\text{O}(100):\text{Cu}$ surface than on the Cu atoms in the bulk. Furthermore, the calculated Bader charges suggest that not the same amount of charge is transferred from each of the outermost Cu atoms (0.3 or 0.2 e).

At the O-terminated $\text{Cu}_2\text{O}(100):\text{O}$ surface, the charges of both the outermost Cu and the outermost O atoms differ from the respective bulk values. While the charge of the coordinatively unsaturated O atoms equals -0.7 e, the charge of the outermost Cu atoms equals 0.6 e. Accordingly, fewer electrons are localized on the outermost O and Cu atoms than on the respective atoms in the bulk (10.4 instead of 10.5 electrons for Cu and 6.7 instead of 7.0 electrons for O). Hence, there is a general lack of electrons at the $\text{Cu}_2\text{O}(100):\text{O}$ surface compared to the Cu_2O bulk phase.

A similar behavior was also observed for the other Cu_2O surfaces, as shown in Figure S6 in the Supporting Information. While the surfaces with an excess of Cu generally have an excess of electrons at the surface compared to those in the bulk phase, the surfaces with an excess of O atoms exhibit a surface electron deficit compared to those in the bulk. For the Cu_2O bulk phase as well as the $\text{Cu}_2\text{O}(111):\text{Cu}$ and $\text{Cu}_2\text{O}(111):\text{Cu/O}$ surfaces, similar values for the Bader net atomic charges have been published.^{26,27,51}

The results above raise the following questions.

1. How can the surface magnetism of Cu_2O surfaces with an excess of oxygen be explained? According to the Bader charge analysis, fewer electrons are localized at the outermost O and Cu atoms of the O-excess Cu_2O surfaces than at the respective atoms in the bulk. This implies that the $3d$ and $2p$ electron orbitals of these outermost Cu and O atoms are not completely occupied. We, therefore, assume that the unpaired $2p$ and $3d$ electrons of the outermost O or Cu atoms lead to the observed local magnetic moments and, thus, to the surface magnetism.
2. Why is the FM arrangement of the magnetic moments the most favorable for the O-excess Cu_2O surfaces? We assume that unpaired electrons at the surface interact with each other and that this exchange interaction causes an energetic splitting of the spin-up/spin-down states (see Figure 4). According to the Stoner theory,^{52,53} such an energetic splitting leads to a redistribution of spin-up electrons into spin-down states and, therefore, an increase in kinetic energy for the redistributed electrons. In some metals, however, this increase in kinetic energy is countered by a decrease in potential energy due to the FM exchange interaction of parallel aligned electron spins. This leads to an overall decrease in energy and, therefore, a FM ground state. We suggest that the observed surface ferromagnetism of O-excess Cu_2O surfaces can be explained in a similar way. Yu et al.¹⁷ and Soon et al.²⁴

also proposed that the origin of the surface ferromagnetism of Cu_2O can be understood within the framework of Stoner's theory.

3. Why do the Cu-excess Cu_2O surfaces not exhibit surface magnetism? According to the Bader charge analysis, more electrons are localized on the outermost Cu atoms of the Cu-excess Cu_2O surfaces than on the respective atoms in the bulk phase. We assume that these additional electrons are localized in the $4s$ orbital, which is in line with our DOS analyses shown in the Supporting Information (Figure S4). Due to the spherical symmetry and nuclear proximity of the $4s$ orbital, these electrons experience a uniform electric field and a high coulomb force. Moreover, the electrons in the $4s$ orbital are shielded from the outside by the fully occupied $3d$ orbitals. Accordingly, we hypothesize that these unpaired $4s$ electrons do not have a strong influence on the magnetic moment of the respective Cu atoms, and thus, the Cu-excess surfaces do not exhibit surface magnetism.

Low-Index CuO Surfaces. Surface Structures. Similar to the Cu_2O system described above, we also investigated all possible surface terminations of the low-index (100), (110), and (111) surfaces of CuO. The fully relaxed surfaces are shown in Figure 6 and in a slightly different perspective in the Supporting Information (Figure S7).

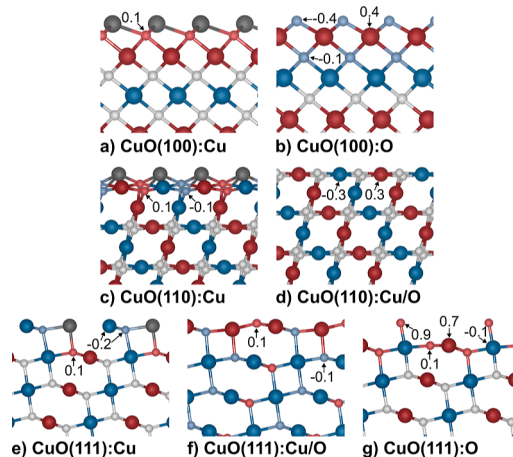


Figure 6. Side views of the calculated low-index CuO surfaces in their most stable magnetic structure. (a) $\text{CuO}(100):\text{Cu}$, (b) $\text{CuO}(100):\text{O}$, (c) $\text{CuO}(110):\text{Cu}$, (d) $\text{CuO}(110):\text{Cu/O}$, (e) $\text{CuO}(111):\text{Cu}$, (f) $\text{CuO}(111):\text{Cu/O}$, and (g) $\text{CuO}(111):\text{O}$. Oxygen atoms and copper atoms are represented by small or large spheres, respectively. Atoms without a magnetic moment are shown in gray, while atoms with a magnetic moment are represented in red (up) or blue (down), depending on the orientation of the local magnetic moments.

Along the $[100]$ direction, CuO is composed of alternating O and Cu layers. Two surface terminations result from this layering: the Cu-terminated $\text{CuO}(100):\text{Cu}$ surface and the O-terminated $\text{CuO}(100):\text{O}$ surface. On the Cu-terminated $\text{CuO}(100):\text{Cu}$ surface, shown in Figure 6a, the outermost Cu atoms are coordinated with three O atoms instead of four as in the bulk. These coordinatively unsaturated Cu atoms shift perpendicular to the surface, resulting in different Cu–O bond lengths. Two of these three Cu–O bonds have a length of 1.98 Å, which is close to the bulk value, while the third one is elongated by 13% to a value of 2.22 Å. On the O-terminated $\text{CuO}(100):\text{O}$ surface, the surface O atoms are coordinated with

only two Cu atoms, which is shown in Figure 6b. These coordinatively unsaturated O atoms relax to the neighboring Cu atoms, which leads to a shortening of the Cu–O bond by 6% (1.83 Å) compared to that of the respective bulk phase.

The (110) surface can be either Cu-terminated or mixed-terminated. Similar to the CuO(100):Cu surface, the outermost Cu atoms on the Cu-terminated CuO(110):Cu surface are coordinated with three O atoms and shift perpendicular to the surface, as represented in Figure 6c. The resulting Cu–O bond distances are 1.99, 2.00, and 2.16 Å, respectively. Only moderate relaxation effects are apparent on the mixed-terminated CuO(110):Cu/O surface, as shown in Figure 6d. The bond distance between coordinatively saturated Cu and coordinatively unsaturated O atoms at the outermost surface layer is shortened by around 4% compared to the bulk value.

Along the [111] direction, three different surface terminations are possible, namely, the Cu-terminated CuO(111):Cu surface, the mixed-terminated CuO(111):Cu/O surface, and the O-terminated CuO(111):O surface. For all three surfaces, only moderate relaxation effects were observed, as shown in Figure 6e–g. On the CuO(111):Cu surface, all O atoms are coordinatively saturated, while the Cu atoms in the outermost surface layer are each bonded with only two O atoms and thus are coordinatively unsaturated. The respective Cu–O distances are 1.89 and 2.02 Å, which corresponds to a 4% change compared to that of the bulk. In the case of the stoichiometric CuO(111):Cu/O surface, half of the Cu and O surface atoms are coordinatively saturated, while the other half are coordinatively unsaturated, having three nearest neighbors. The corresponding Cu–O bond lengths are between 1.85 and 2.00 Å. On the CuO(111):O surface, all Cu atoms on the surface are coordinatively saturated, while the O atoms are surrounded by either one, three, or four Cu atoms. The Cu–O bond to the outermost O atom is shortened by 11% (1.74 Å) compared to that of the bulk, while the other Cu–O distances are between 1.86 and 2.02 Å.

Surface Magnetism. Similar to Cu₂O, all investigated CuO surfaces have either an excess of Cu or O atoms, except for the stoichiometric CuO(111):Cu/O surface. This excess of Cu or O atoms can be described with the stoichiometric ratio $R_{\text{Cu/O}}$ (as described above), where a value larger than one indicates an excess of Cu atoms and a value smaller than one indicates an excess of O atoms on the surface. The corresponding $R_{\text{Cu/O}}$ values for all calculated CuO surfaces are given in Table 2.

As for the Cu₂O surfaces, there seems to be a correlation between the stoichiometric ratio $R_{\text{Cu/O}}$ and the magnetic moments of the surface atoms, which are represented by different colors in Figure 6. If there is an excess of Cu atoms on the surface ($R_{\text{Cu/O}} > 1$), as in CuO(100):Cu, CuO(110):Cu, and CuO(111):Cu, all or some of the outermost Cu atoms do not have a magnetic moment, although all the bulk-like Cu atoms have a magnetic moment, as in CuO itself. On the other hand, if there is an excess of O atoms on the surface ($R_{\text{Cu/O}} < 1$), the outermost Cu atoms have a magnetic moment, which is lower than that in the bulk, e.g., $0.4 \mu_{\text{B}}$ for CuO(100):O, $0.3 \mu_{\text{B}}$ for CuO(110):Cu/O, and $0.1 \mu_{\text{B}}$ for the Cu atoms coordinated with the outermost O atoms on the CuO(111):O surface.

In the case of CuO(100):O and CuO(111):O, the oxygen surface atoms additionally have a magnetic moment of $0.4 \mu_{\text{B}}$ in the first surface layer and $0.1 \mu_{\text{B}}$ in the second O-layer for CuO(100):O, and $0.9 \mu_{\text{B}}$ in the first and $0.1 \mu_{\text{B}}$ in the second O-layer for CuO(111):O. For the stoichiometric CuO(111):Cu/O surface ($R_{\text{Cu/O}} = 1$), all O atoms in the corresponding

supercell have a magnetic moment around $0.1 \mu_{\text{B}}$, as opposed to only those located directly at the surface.

Within the most stable magnetic structure, the arrangement of the magnetic moments of the bulk-like atoms along the [100] and [110] directions is independent of the respective surface termination, as shown in Figure 6a–d. Both CuO(100):Cu and CuO(100):O show a layer-by-layer ordering of the local magnetic moments, while CuO(110):Cu and CuO(110):Cu/O favor a line-by-line ordering. However, along the [111] direction, the mixed termination shows a different magnetic structure than the other terminations, as illustrated by the different colors in Figure 6e–g. Similar to the (110) surfaces, the CuO(111):Cu and CuO(111):O surfaces show a line-by-line ordering of the magnetic moments, whereas CuO(111):Cu/O favors a so-called bulk-like spin ordering. Here, the magnetic moments alternate along the surface plane, as shown in a slightly different perspective in the Supporting Information (Figure S7).

In addition to the most stable AFM configuration described above, various other magnetic structures have been studied as well. Here, one DM, one FM, and several AFM configurations were obtained for each CuO surface. The corresponding surface energies of the most stable FM, AFM, and DM configurations, respectively, are summarized in Figure 7, while their surface

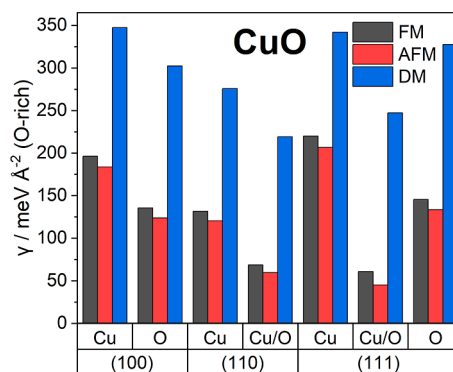


Figure 7. Surface energies for different magnetic configurations of low-index CuO surfaces. The FM, AFM, and DM configurations are indicated in black, red, and blue, respectively.

structures for the overall most stable magnetic configuration are presented in Figure 6. As shown in Figure 7, for all investigated CuO surfaces, the AFM structure has the lowest surface energy and is, therefore, considered to be the most stable. The DM structures are in all cases the least stable ones. Similar to Cu₂O, the energy difference between AFM and DM is most pronounced for the overall most stable CuO(111):Cu/O surface. In contrast to Cu₂O, the energy difference between AFM and FM is also the largest for the most stable surface.

The calculated structural and magnetic properties of the CuO(111):Cu/O surface agree well with other theoretical studies.^{22,28,54,55} However, to the best of our knowledge, no structural and magnetic properties of the polar nonstoichiometric CuO surfaces investigated in this study were reported previously.

Electronic Properties. The electronic properties of the CuO surfaces were deduced from the calculated spin-polarized DOS. The total, partial, and projected DOS of the most stable CuO(111):Cu/O surface are shown in Figure 8, while the DOS for the other surfaces is given in the Supporting Information (see Figures S8 and S9).

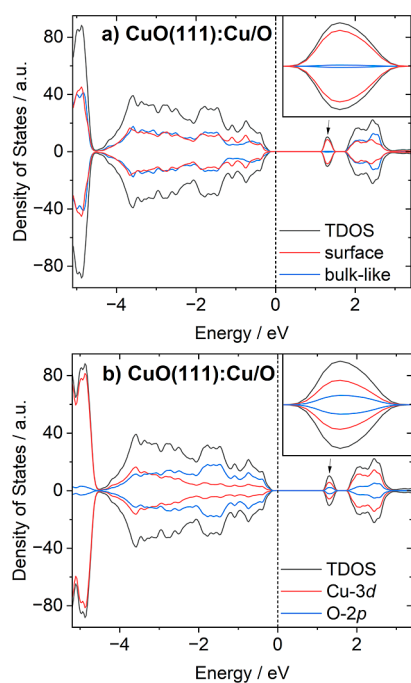


Figure 8. Partial (a) and projected (b) DOS of the CuO(111):Cu/O surface. The TDOS is shown in gray. The contribution of the surface atoms (outermost atom layers) and the Cu-3*d* orbitals are shown in red, while the contribution of all other (bulk-like) atoms in the calculated cell and the O-2*p* orbitals are represented in blue. The Fermi energy is indicated by a vertical black line at 0 eV.

For the stoichiometric CuO(111):Cu/O surface, there is no difference between the DOS for spin-up electrons (plotted upward) and the DOS for spin-down electrons (plotted downward). Compared to the CuO bulk phase, additional states are observed near the conduction band minimum (around 1.3 eV), which are magnified in the inset. These states can be attributed to the surface atoms and exhibit both Cu-3*d* and O-2*p* characters, with the density of the Cu-3*d* states being greater than the density of the O-2*p* states.

Similar to the Cu₂O(100):O surface, this 2*p*-3*d* hybridization can be observed not only for the surface atoms but also in the bulk. The projected DOS shows that the states from -4.5 eV to the valence band maximum have both O-2*p* and Cu-3*d* contributions. However, the density of the Cu states decreases in this range, while the density of the O states remains almost constant. Consequently, the states above -2 eV can be assigned predominantly to the O-2*p* orbitals. On the other hand, the states below -4.5 eV are almost exclusively related to Cu-3*d* states.

Similar to the CuO(111):Cu/O surface, the DOS for the CuO(100):Cu, CuO(110):Cu, and CuO(110):Cu/O surfaces, as well as for the CuO bulk phase, show a nearly identical shape for spin-up and spin-down states and accordingly no spin polarization. In contrast, the DOS for the CuO(111):Cu, CuO(100):O, and CuO(111):O surfaces show different characteristics for spin-up and spin-down electrons. A possible reason for this behavior could be the sum of the magnetic moments of the atoms in the respective supercells. While the net magnetic moments of the CuO(111):Cu/O, CuO(100):Cu, CuO(110):Cu, and CuO(110):Cu/O supercells is zero, the sum of the magnetic moments of all atoms in CuO(111):Cu, CuO(100):O, and CuO(111):O is nonzero. This indicates that the CuO(111):Cu, CuO(100):O and CuO(111):O surfaces

have either an excess of spin-down or spin-up electrons at the surface, which can also be deduced from Figure 6. Therefore, the respective DOS show different characteristics for spin-up and spin-down electrons.

To gain further insights into the electronic structure of the surface atoms, we additionally performed a Bader charge analysis for all investigated CuO surfaces, as shown in the Supporting Information (Figure S10). For all surfaces, the charge of the atoms inside the slabs matches the charge of the respective atoms in the bulk phase, namely, 1.1 e for Cu and -1.1 e for O atoms, respectively. In the bulk phase, as well as inside the slabs, each Cu atom is coordinated with four O atoms, and each O atom is coordinated with four Cu atoms. This indicates that on average 0.275 e is transferred from each Cu atom to each neighboring O atom.

For the Cu-terminated surfaces, the calculated Bader charges of the outermost Cu atoms are about 0.5 e. Accordingly, the charge of the outermost Cu atoms of these CuO surfaces is similar to the charge of the Cu atoms in the Cu₂O bulk phase. This indicates that the outermost Cu atoms of the Cu-terminated CuO surfaces are reduced (from Cu²⁺ to Cu⁺). This interpretation is in line with Maimaiti et al., who also suggested that a change in charge of 0.5–0.6 e indicates a reduction from Cu²⁺ to Cu⁺.⁵⁴

For the O-terminated surfaces, only the charges of the outermost O atoms differ from the respective bulk values. Although there is a deficiency of electrons on the O-excess CuO surfaces compared to the CuO bulk phase, the charge of the Cu atoms does not change compared to those in the bulk phase. This indicates that the Cu atoms transfer a maximum of 1.1 e regardless of their coordination environment, and thus, none of the Cu atoms have an oxidation state larger than that in CuO.

Energetics and Thermodynamics. The stability of the copper oxide surfaces was investigated using the ab initio atomistic thermodynamics approach.^{22,25,26,56} Assuming the system to be in contact with a Cu-bulk and a gaseous oxygen reservoir, the temperature *T*- and pressure *p*-dependent surface energy of the Cu₂O ($\gamma^{\text{Cu}_2\text{O}}$) and CuO (γ^{CuO}) surfaces can be calculated using

$$\begin{aligned} \gamma^{\text{Cu}_2\text{O}}(T, p) = & \frac{1}{2A} \{ G^{\text{slab}}(T, p, N_{\text{Cu}}, N_{\text{O}}) \\ & - \frac{1}{2} N_{\text{Cu}} g_{\text{Cu}_2\text{O}}^{\text{bulk}}(T, p) \\ & + \left(\frac{1}{2} N_{\text{Cu}} - N_{\text{O}} \right) \mu_{\text{O}}(T, p) \} \end{aligned} \quad (1)$$

and

$$\begin{aligned} \gamma^{\text{CuO}}(T, p) = & \frac{1}{2A} \{ G^{\text{slab}}(T, p, N_{\text{Cu}}, N_{\text{O}}) \\ & - N_{\text{Cu}} g_{\text{CuO}}^{\text{bulk}}(T, p) \\ & + (N_{\text{Cu}} - N_{\text{O}}) \mu_{\text{O}}(T, p) \}, \end{aligned} \quad (2)$$

where *A* is the area of the surface unit cell, G^{slab} is the Gibbs free energy of the surface slab containing a certain number of Cu atoms N_{Cu} and O atoms N_{O} , and g^{bulk} is the Gibbs free energy per formula unit of the respective bulk phase. The oxygen chemical potential μ_{O} can only be varied within certain boundaries,^{25,56} which are given by

$$\Delta_f G(0, 0) < \Delta\mu_{\text{O}}(T, p) < 0 \quad (3)$$

where μ_{O} is referenced to the total energy of an O atom in molecular oxygen, $\Delta\mu_{\text{O}}(T, p) = \mu_{\text{O}}(T, p) - \frac{1}{2}E_{\text{O}_2}^{\text{total}}$, and $\Delta_f G(0, 0)$ is the Gibbs free energy of formation per formula unit of the respective bulk oxide, i.e., Cu_2O or CuO . The lower boundary of eq 3 is called the oxygen-poor (O-poor) limit, while the upper boundary is referred to as the oxygen-rich (O-rich) limit. By assuming that the contributions of the pV -term as well as the complete vibrational contribution to the Gibbs free energy can be neglected, the Gibbs free energies in eqs 1 and 2 can be approximated by total energies extracted from DFT calculations.^{26,56} This allows rewriting eqs 1 and 2 as

$$\begin{aligned} \gamma^{\text{Cu}_2\text{O}}(T, p) = & \frac{1}{2A} \{ E^{\text{slab}}(V, N_{\text{Cu}}, N_{\text{O}}) \\ & - \frac{1}{2} N_{\text{Cu}} E_{\text{Cu}_2\text{O}}^{\text{bulk}}(V) \\ & + \left(\frac{1}{2} N_{\text{Cu}} - N_{\text{O}} \right) \Delta\mu_{\text{O}}(T, p) \} \end{aligned} \quad (4)$$

and

$$\begin{aligned} \gamma^{\text{CuO}}(T, p) = & \frac{1}{2A} \{ E^{\text{slab}}(V, N_{\text{Cu}}, N_{\text{O}}) \\ & - N_{\text{Cu}} E_{\text{CuO}}^{\text{bulk}}(V) \\ & + (N_{\text{Cu}} - N_{\text{O}}) \Delta\mu_{\text{O}}(T, p) \}, \end{aligned} \quad (5)$$

which only contain terms directly obtainable from DFT calculations. Using eqs 4 and 5, we calculated the surface energy γ of all copper oxide surfaces in their most stable magnetic configuration under O-poor and O-rich conditions. The corresponding values are given in Table 2. Here, a lower surface energy implies a thermodynamically more stable surface. If there is an excess of Cu atoms at the surface, e.g., $R_{\text{Cu/O}} > 2$ for Cu_2O or $R_{\text{Cu/O}} > 1$ for CuO , the surface energy has a lower value under O-poor than under O-rich conditions, which means that the Cu-excess surfaces are more stable under O-poor conditions. On the other hand, if there is an excess of oxygen atoms at the surface, e.g., $R_{\text{Cu/O}} < 2$ for Cu_2O or $R_{\text{Cu/O}} < 1$ for CuO , the surface is more stable under O-rich conditions. For the stoichiometric $\text{Cu}_2\text{O}(111):\text{Cu/O}$ and $\text{CuO}(111):\text{Cu/O}$ slabs, the surface energy under O-rich and O-poor conditions is identical, i.e., the surface energy is independent of the oxygen chemical potential.

These correlations can also be observed in the surface phase diagrams shown in Figure 9, which illustrates the surface energy as a function of the oxygen chemical potential. While the surface energy of the stoichiometric surfaces is constant in the surface phase diagram, the surface energy of the Cu-excess surfaces increases with increasing oxygen chemical potential and the surface energy of the O-excess surfaces decreases with increasing oxygen chemical potential.

Comparing the surface energies of the low-index Cu_2O surfaces, as shown in Figure 9a, it becomes apparent that there is a “competition” in stability between the $\text{Cu}_2\text{O}(111):\text{Cu/O}$, $\text{Cu}_2\text{O}(110):\text{Cu/O}$, and $\text{Cu}_2\text{O}(111):\text{O}$ surfaces. The surface phase diagram further indicates that the stoichiometric $\text{Cu}_2\text{O}(111):\text{Cu/O}$ surface is the most stable one above the O-poor limit. However, with increasing oxygen chemical potential ($\Delta\mu_{\text{O}} > -1.3$ eV), the mixed-terminated $\text{Cu}_2\text{O}(110):\text{Cu/O}$ becomes

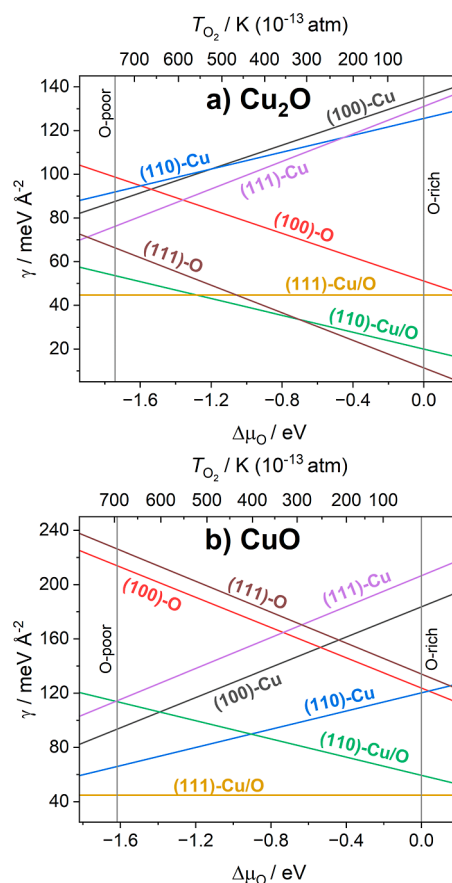


Figure 9. Calculated surface free energy of various Cu_2O (a) and CuO (b) surfaces as a function of the oxygen chemical potential $\Delta\mu_{\text{O}}$. The corresponding temperature at a pressure of 10^{-13} atm is given in the top x axis.

more stable until the O-terminated $\text{Cu}_2\text{O}(111):\text{O}$ surface is the most stable around the O-poor limit ($\Delta\mu_{\text{O}} > -0.7$ eV).

In contrast, the surface phase diagram for the low-index CuO surfaces indicates that the stoichiometric $\text{CuO}(111):\text{Cu/O}$ surface is the most stable over the whole oxygen chemical potential range. To clarify the physical meaning of this range of oxygen chemical potential, we calculated the corresponding temperature of the surrounding oxygen atmosphere at UHV conditions. The resulting temperature scale is shown in the top x axis of Figure 9.

For the Cu_2O surfaces, a similar trend in the surface phase diagram was reported by Soon et al.^{25,29} Furthermore, the calculated surface energies for the $\text{Cu}_2\text{O}(100):\text{O}$, $\text{Cu}_2\text{O}(110):\text{Cu}$, $\text{Cu}_2\text{O}(110):\text{Cu/O}$, and $\text{Cu}_2\text{O}(111):\text{Cu/O}$ surfaces under O-rich and O-poor conditions, as well as their progression in the phase diagram, are in excellent agreement with those reported by Bendavid et al.,²⁶ whose studies are also based on PBE + U calculations. For the stoichiometric $\text{Cu}_2\text{O}(111):\text{Cu/O}$ surface, several values of the surface energy have been published, and the surface energy calculated in our study is in the range of the reported values of $0.67\text{--}0.78$ J m^{-2} ($42\text{--}49$ $\text{meV } \text{Å}^{-2}$).^{25–27,29,57}

The calculated surface energy for the stoichiometric $\text{CuO}(111):\text{Cu/O}$ surface is in excellent agreement with Hu et al. (46 $\text{meV } \text{Å}^{-2}$)²² and Mishra et al. (47 $\text{meV } \text{Å}^{-2}$).²⁸ Furthermore, in both studies, $\text{CuO}(111):\text{Cu/O}$ is identified as the most stable CuO surface, which is also in line with our investigations.^{22,28} However, to the best of our knowledge, only

a few surface energies have been reported for the nonstoichiometric CuO surfaces. Hu et al.²² reported a surface phase diagram for the nonstoichiometric CuO(110):Cu and CuO(110):O surfaces but did not include the corresponding surface structures. Therefore, a comparison of the phase diagrams is not readily possible. Nevertheless, the surface energies under O-poor and O-rich conditions for the nonstoichiometric CuO(110):Cu surface are in very good agreement with our calculations.

CONCLUSIONS

Using PBE + *U*, we have investigated the structural and magnetic properties of low-index Cu₂O and CuO surfaces as well as their bulk oxides. Comparing various possible spin configurations, we found that CuO prefers being AFM, while for Cu₂O, the DM configuration is most stable.

For the low-index Cu₂O surfaces, we observed a correlation between the stoichiometric ratio $R_{\text{Cu/O}}$ and the magnetic moments of the surface atoms. If there is an excess of oxygen atoms on the surface, the surface atoms have a magnetic moment with the FM structure being the most stable. Otherwise, the respective surfaces are DM as the Cu₂O oxide itself.

In order to investigate the observed surface ferromagnetism in more detail, we calculated the spin-polarized DOS and performed a Bader charge analysis. According to the Bader charge analysis, fewer electrons are localized at the outermost O and Cu atoms of the O-excess Cu₂O surfaces than at the respective atoms in the bulk. Furthermore, the spin-polarized DOS of the O-excess Cu₂O surfaces shows additional spin-down states near the Fermi level or the conduction band minimum. Therefore, we assume that the unpaired 2*p* and 3*d* electrons of the outermost O and Cu atoms interact with each other, which causes the energetic splitting of the spin-up/spin-down states observed in the DOS. We further suggest that the FM exchange interaction of parallel-aligned electron spins leads to an overall decrease in energy and therefore to the observed surface ferromagnetism of the O-excess Cu₂O surfaces.

Similar to Cu₂O, we observed a correlation between the stoichiometric ratio and the magnetic moments of the surface atoms for the low-index CuO surfaces. If there is an excess of copper atoms on the surface, all or some of the outermost Cu atoms have no magnetic moment, although all the bulk-like Cu atoms have a magnetic moment, as in CuO itself. On the other hand, if there is an excess of oxygen atoms on the surface, the outermost Cu atoms have a magnetic moment, which is lower than that in the bulk phase. To shed light on the magnetic properties of the different terminated low-index CuO surfaces, we analyzed their electronic structure including the Bader charges of the respective atoms. The Bader charge analysis of the CuO surfaces shows that the charge of the outermost Cu atoms of the Cu-terminated CuO surfaces is similar to the charge of the Cu atoms in the Cu₂O bulk phase, which indicates that these Cu atoms are reduced (from Cu²⁺ to Cu⁺). We assume this is the reason why the outermost Cu atoms of the Cu-terminated CuO surfaces have no unpaired 3*d* electrons and, accordingly, no magnetic moment.

To study the stability of the copper oxide surfaces, we used the ab initio atomistic thermodynamics approach. The resulting surface phase diagram for the Cu₂O surfaces indicates that there is a competition in stability between the Cu₂O(111):Cu/O, Cu₂O(110):Cu/O, and Cu₂O(111):O surfaces, while the surface phase diagram for the CuO surfaces reveals that the

stoichiometric CuO(111):Cu/O surface is the most stable CuO surface over the whole range of oxygen chemical potentials.

In conclusion, we presented a correlation between the structural and magnetic properties of different terminated copper oxide surfaces and offered a possible explanation for the observed magnetism within a simplified model. In addition, this work offers insights into the surface structure of copper-based catalysts and forms the basis for further investigations of catalytic reactions on copper oxide surfaces.

ASSOCIATED CONTENT

Data Availability Statement

The data supporting the findings of this study are openly available in Zenodo at [10.5281/zenodo.10653474](https://doi.org/10.5281/zenodo.10653474).

Supporting Information

The Supporting Information is available free of charge at <https://pubs.acs.org/doi/10.1021/acs.jpcc.4c01102>.

Bulk properties for various values of the *U* parameter, structure of three possible AFM orderings in CuO, DOS of Cu₂O and CuO, Bader charge analysis of Cu₂O and CuO, structure of the Cu₂O and CuO surfaces from another perspective, DOS of the Cu₂O and CuO surfaces, and Bader charge analysis of the Cu₂O and CuO surfaces (PDF)

AUTHOR INFORMATION

Corresponding Author

Timo Jacob – Institute of Electrochemistry, Ulm University, 89081 Ulm, Germany; Helmholtz-Institute Ulm (HIU) for Electrochemical Energy Storage, 89081 Ulm, Germany; Karlsruhe Institute of Technology (KIT), 76021 Karlsruhe, Germany; orcid.org/0000-0001-7777-2306; Email: timo.jacob@uni-ulm.de

Authors

Stefanie E. Bogenrieder – Institute of Electrochemistry, Ulm University, 89081 Ulm, Germany; orcid.org/0009-0006-9201-4486

Julian Beßner – Institute of Electrochemistry, Ulm University, 89081 Ulm, Germany; orcid.org/0000-0001-9454-3679

Albert K. Engstfeld – Institute of Electrochemistry, Ulm University, 89081 Ulm, Germany; orcid.org/0000-0002-9686-3948

Complete contact information is available at: <https://pubs.acs.org/10.1021/acs.jpcc.4c01102>

Author Contributions

S. E. Bogenrieder: conceptualization, investigation, data generation and analysis, visualization, and writing—original draft preparation. J. Beßner: writing—review and editing. A. K. Engstfeld: writing—review and editing. T. Jacob: resources, supervision, and writing—review and editing.

Notes

The authors declare no competing financial interest.

ACKNOWLEDGMENTS

The authors acknowledge support by the state of Baden-Württemberg through bwHPC and the German Research Foundation (DFG) through grant no. INST 40/575-1 FUGG (JUSTUS 2 cluster). Additional simulations were performed on the high-performance computing cluster ULMIX provided by the Institute of Electrochemistry at Ulm University. Further-

more, support from the DFG through the priority programs SPP-2370 (project 502202153), the collaborative research centre SFB-1316 (project 327886311), and project 501805371 is gratefully acknowledged. Finally, we thank Dr. Björn Kirchoff for his support and valuable discussions.

REFERENCES

- (1) Zoofakar, A. S.; Rani, R. A.; Morfa, A. J.; O'Mullane, A. P.; Kalantar-zadeh, K. Nanostructured copper oxide semiconductors: a perspective on materials, synthesis methods and applications. *J. Mater. Chem. C* **2014**, *2*, 5247–5270.
- (2) Giziński, D.; Brudzisz, A.; Santos, J. S.; Trivinho-Strixino, F.; Stepiński, W. J.; Czujko, T. Nanostructured Anodic Copper Oxides as Catalysts in Electrochemical and Photoelectrochemical Reactions. *Catalysts* **2020**, *10*, 1338.
- (3) Rydosz, A. The Use of Copper Oxide Thin Films in Gas-Sensing Applications. *Coatings* **2018**, *8*, 425.
- (4) Majumdar, D.; Ghosh, S. Recent advancements of copper oxide based nanomaterials for supercapacitor applications. *J. Energy Storage* **2021**, *34*, 101995.
- (5) Chakraborty, N.; Banerjee, J.; Chakraborty, P.; Banerjee, A.; Chanda, S.; Ray, K.; Acharya, K.; Sarkar, J. Green synthesis of copper/copper oxide nanoparticles and their applications: a review. *Green Chem. Lett. Rev.* **2022**, *15*, 187–215.
- (6) Baranov, A.; Mishra, V.; Pandey, P.; Rao, M. S. R.; Dixit, T. Investigations Into the Role of Native Defects on Photovoltaic and Spintronic Properties in Copper Oxide. *IEEE Trans. Nanotechnol.* **2022**, *21*, 522–527.
- (7) Niluis, N.; Goniakowski, J.; Noguera, C. A surface science view onto cuprous oxide: Growth, termination, electronic structure and optical response. *Surf. Sci. Rep.* **2024**, *79*, 100622.
- (8) Baranov, O.; Bazaka, K.; Belmonte, T.; Riccardi, C.; Roman, H. E.; Mohandas, M.; Xu, S.; Cvelbar, U.; Levchenko, I. Recent innovations in the technology and applications of low-dimensional CuO nanostructures for sensing, energy and catalysis. *Nanoscale Horiz.* **2023**, *8*, 568–602.
- (9) Steinhauer, S. Gas Sensors Based on Copper Oxide Nanomaterials: A Review. *Chemosensors* **2021**, *9*, 51.
- (10) Wang, Y.; Pierson, J. F. Binary copper oxides as photovoltaic absorbers: recent progress in materials and applications. *J. Phys. D: Appl. Phys.* **2021**, *54*, 263002.
- (11) Bagal, I. V.; Chodankar, N. R.; Hassan, M. A.; Waseem, A.; Johar, M. A.; Kim, D.-H.; Ryu, S.-W. Cu₂O as an emerging photocathode for solar water splitting - A status review. *Int. J. Hydrogen Energy* **2019**, *44*, 21351–21378.
- (12) Gattinoni, C.; Michaelides, A. Atomistic details of oxide surfaces and surface oxidation: the example of copper and its oxides. *Surf. Sci. Rep.* **2015**, *70*, 424–447.
- (13) Jang, Y. J.; Lindberg, A. E.; Lumley, M. A.; Choi, K.-S. Photoelectrochemical Nitrogen Reduction to Ammonia on Cupric and Cuprous Oxide Photocathodes. *ACS Energy Lett.* **2020**, *5*, 1834–1839.
- (14) Shih, P.-H.; Ji, J.-Y.; Ma, Y.-R.; Wu, S. Y. Size effect of surface magnetic anisotropy in Cu₂O nanoparticles. *J. Appl. Phys.* **2008**, *103*, 07B735.
- (15) Prabhakaran, G.; Murugan, R. Room temperature ferromagnetic properties of Cu₂O microcrystals. *J. Alloys Compd.* **2013**, *579*, 572–575.
- (16) Chen, C.; He, L.; Lai, L.; Zhang, H.; Lu, J.; Guo, L.; Li, Y. Magnetic properties of undoped Cu₂O fine powders with magnetic impurities and/or cation vacancies. *J. Phys.: Condens. Matter* **2009**, *21*, 145601.
- (17) Yu, X.; Zhang, X.; Wang, S.; Feng, G. A first principle study on the magnetic properties of Cu₂O surfaces. *Curr. Appl. Phys.* **2015**, *15*, 1303–1311.
- (18) Gao, D.; Zhang, J.; Zhu, J.; Qi, J.; Zhang, Z.; Sui, W.; Shi, H.; Xue, D. Vacancy-Mediated Magnetism in Pure Copper Oxide Nanoparticles. *Nanoscale Res. Lett.* **2010**, *5*, 769–772.
- (19) Karthik, K.; Victor Jaya, N.; Kanagaraj, M.; Arumugam, S. Temperature-dependent magnetic anomalies of CuO nanoparticles. *Solid State Commun.* **2011**, *151*, 564–568.
- (20) Rao, G.; Yao, Y.; Chen, J. Superparamagnetic behavior of antiferromagnetic CuO nanoparticles. *IEEE Trans. Magn.* **2005**, *41*, 3409–3411.
- (21) Rehman, S.; Mumtaz, A.; Hasanain, S. K. Size effects on the magnetic and optical properties of CuO nanoparticles. *J. Nanopart. Res.* **2011**, *13*, 2497–2507.
- (22) Hu, J.; Li, D.; Lu, J. G.; Wu, R. Effects on Electronic Properties of Molecule Adsorption on CuO Surfaces and Nanowires. *J. Phys. Chem. C* **2010**, *114*, 17120–17126.
- (23) Das, R.; Alonso, J.; Jefremovas, E. M.; Fernández Barquín, L.; Ngoc, P. K.; Nguyen, H. T.; Viet, D. T.; Vinh, P. V.; Duong, A. T. Suppression of ferromagnetic order in CuO/Cu₂O nanocomposites. *Mater. Today Commun.* **2022**, *32*, 104038.
- (24) Soon, A.; Cui, X.-Y.; Delley, B.; Wei, S.-H.; Stampfl, C. Native defect-induced multifarious magnetism in nonstoichiometric cuprous oxide: First-principles study of bulk and surface properties of Cu_{2-δ}O. *Phys. Rev. B* **2009**, *79*, 035205.
- (25) Soon, A.; Todorova, M.; Delley, B.; Stampfl, C. Thermodynamic stability and structure of copper oxide surfaces: A first-principles investigation. *Phys. Rev. B* **2007**, *75*, 125420.
- (26) Bendavid, L. I.; Carter, E. A. First-Principles Predictions of the Structure, Stability, and Photocatalytic Potential of Cu₂O Surfaces. *J. Phys. Chem. B* **2013**, *117*, 15750–15760.
- (27) Islam, M. M.; Diawara, B.; Maurice, V.; Marcus, P. Bulk and surface properties of Cu₂O: A first-principles investigation. *J. Mol. Struct. THEOCHEM* **2009**, *903*, 41–48.
- (28) Mishra, A. K.; Roldan, A.; de Leeuw, N. H. CuO Surfaces and CO₂ Activation: A Dispersion-Corrected DFT+U Study. *J. Phys. Chem. C* **2016**, *120*, 2198–2214.
- (29) Soon, A.; Todorova, M.; Delley, B.; Stampfl, C. Erratum: Thermodynamic stability and structure of copper oxide surfaces: A first-principles investigation. *Phys. Rev. B* **2007**, *75*, 125420. *Physical Review B* **2007**, *76*, 129902
- (30) Telegin, A.; Sukhorukov, Y. Magnetic Semiconductors as Materials for Spintronics. *Magnetochemistry* **2022**, *8*, 173.
- (31) Kresse, G.; Furthmüller, J. Efficiency of ab-initio total energy calculations for metals and semiconductors using a plane-wave basis set. *Comput. Mater. Sci.* **1996**, *6*, 15–50.
- (32) Kresse, G.; Furthmüller, J. Efficient iterative schemes for ab initio total-energy calculations using a plane-wave basis set. *Phys. Rev. B* **1996**, *54*, 11169–11186.
- (33) Blöchl, P. E. Projector augmented-wave method. *Phys. Rev. B* **1994**, *50*, 17953–17979.
- (34) Kresse, G.; Joubert, D. From ultrasoft pseudopotentials to the projector augmented-wave method. *Phys. Rev. B* **1999**, *59*, 1758–1775.
- (35) Perdew, J. P.; Burke, K.; Ernzerhof, M. Generalized Gradient Approximation Made Simple. *Phys. Rev. Lett.* **1996**, *77*, 3865–3868.
- (36) Dudarev, S. L.; Botton, G. A.; Savrasov, S. Y.; Humphreys, C. J.; Sutton, A. P. Electron-energy-loss spectra and the structural stability of nickel oxide: An LSDA+U study. *Phys. Rev. B* **1998**, *57*, 1505–1509.
- (37) Živković, A.; Roldan, A.; De Leeuw, N. H. Density functional theory study explaining the underperformance of copper oxides as photovoltaic absorbers. *Phys. Rev. B* **2019**, *99*, 035154.
- (38) Pack, J. D.; Monkhorst, H. J. Special points for Brillouin-zone integrations—a reply. *Phys. Rev. B* **1977**, *16*, 1748–1749.
- (39) Wang, V.; Xu, N.; Liu, J.-C.; Tang, G.; Geng, W.-T. VASPKIT: A user-friendly interface facilitating high-throughput computing and analysis using VASP code. *Comput. Phys. Commun.* **2021**, *267*, 108033.
- (40) Bader, R. F. W. Atoms in molecules. *Acc. Chem. Res.* **1985**, *18*, 9–15.
- (41) Henkelman, G.; Arnaldsson, A.; Jónsson, H. A fast and robust algorithm for Bader decomposition of charge density. *Comput. Mater. Sci.* **2006**, *36*, 354–360.
- (42) Momma, K.; Izumi, F. VESTA 3 for three-dimensional visualization of crystal, volumetric and morphology data. *J. Appl. Crystallogr.* **2011**, *44*, 1272–1276.

- (43) Chase, M. J. NIST-JANAF Thermochemical Tables. *J. Phys. Chem. Ref. Data Monograph* **1998**, *9*, 1–1961.
- (44) Scanlon, D. O.; Morgan, B. J.; Watson, G. W. Modeling the polaronic nature of p-type defects in Cu_2O : The failure of GGA and GGA+U. *J. Chem. Phys.* **2009**, *131*, 124703.
- (45) Meyer, B. K.; Polity, A.; Reppin, D.; Becker, M.; Hering, P.; Klar, P. J.; Sander, T.; Reindl, C.; Benz, J.; Eickhoff, M.; et al. Binary copper oxide semiconductors: From materials towards devices. *Phys. Status Solidi B* **2012**, *249*, 1487–1509.
- (46) Forsyth, J. B.; Brown, P. J.; Wanklyn, B. M. Magnetism in cupric oxide. *J. Phys. C: Solid State Phys.* **1988**, *21*, 2917–2929.
- (47) O'Reilly, D. E. Electronic configuration of metal oxides. *J. Chem. Educ.* **1961**, *38*, 312–316.
- (48) Liao, L.; Yan, B.; Hao, Y. F.; Xing, G. Z.; Liu, J. P.; Zhao, B. C.; Shen, Z. X.; Wu, T.; Wang, L.; Thong, J. T. L.; et al. P-type electrical, photoconductive, and anomalous ferromagnetic properties of Cu_2O nanowires. *Appl. Phys. Lett.* **2009**, *94*, 2–5.
- (49) Nisar, J.; Peng, X.; Ahuja, R. Origin of ferromagnetism in molybdenum dioxide from ab initio calculations. *Phys. Rev. B* **2010**, *81*, 012402.
- (50) Sundaresan, A.; Bhargavi, R.; Rangarajan, N.; Siddesh, U.; Rao, C. N. R. Ferromagnetism as a universal feature of nanoparticles of the otherwise nonmagnetic oxides. *Phys. Rev. B* **2006**, *74*, 161306.
- (51) Laskowski, R.; Blaha, P.; Schwarz, K. Charge distribution and chemical bonding in Cu_2O . *Phys. Rev. B* **2003**, *67*, 075102.
- (52) Stoner, E. C. Collective electron ferromagnetism. *Proc. R. Soc. London, Ser. A* **1938**, *165*, 372–414.
- (53) Stoner, E. C. Collective electron ferromagnetism II. Energy and specific heat. *Proc. R. Soc. London, Ser. A* **1939**, *169*, 339–371.
- (54) Maimaiti, Y.; Nolan, M.; Elliott, S. D. Reduction mechanisms of the $\text{CuO}(111)$ surface through surface oxygen vacancy formation and hydrogen adsorption. *Phys. Chem. Chem. Phys.* **2014**, *16*, 3036.
- (55) Yu, X.; Zhang, X.; Wang, H.; Feng, G. High coverage water adsorption on the $\text{CuO}(111)$ surface. *Appl. Surf. Sci.* **2017**, *425*, 803–810.
- (56) Reuter, K.; Scheffler, M. Composition, structure, and stability of $\text{RuO}_2(110)$ as a function of oxygen pressure. *Phys. Rev. B* **2001**, *65*, 035406.
- (57) Soon, A.; Söhnle, T.; Idriss, H. Plane-wave pseudopotential density functional theory periodic slab calculations of CO adsorption on $\text{Cu}_2\text{O}(111)$ surface. *Surf. Sci.* **2005**, *579*, 131–140.